Journal of Fluids and Structures (2002) **16**(4), 435–451
doi:10.1006/jfls.2001.0429, available online at http://www.idealibrary.com on IDEAL®

NUMERICAL SIMULATION OF FLOW INDUCED BY A CYLINDER ORBITING IN A LARGE VESSEL

I. Teschauer, M. Schäfer and A. Kempf

Department of Numerical Methods in Mechanical Engineering
Darmstadt University of Technology
Petersenstr. 30, D-64287 Darmstadt, Germany

(Received 29 January 1999, and in final form 16 August 2001)

The flow field induced by a circular cylinder orbiting in a large vessel filled with fluid is investigated numerically. A finite-volume method is applied to the two-dimensional incompressible Navier–Stokes equations to compute the unsteady laminar flow fields. Moving reference systems are employed to allow an easy imposition of boundary conditions and to avoid grid deformation. Aspects of numerical accuracy related to the number of grid points and time steps employed are discussed. The flow is governed by two dimensionless parameters: a Reynolds number and a Keulegan–Carpenter number. These are varied systematically in order to find their influence on the flow pattern. In particular, the temporal development of the vorticity field and the lift on the cylinder are examined.

1. INTRODUCTION

The flow around a circular cylinder is one of the classical problems of fluid dynamics. Cylinders in constant cross-flow or moving at constant velocity in a fluid at rest have been the main focus of numerous experimental, theoretical and computational studies [see, e.g., Zdravkovich (1997) and the references therein]. Also, a variety of results for cylinders in periodic cross-flow or translationally oscillating cylinders can be found in the literature [e.g., Dütsch *et al.* (1998), Tatsuno & Bearman (1990), Lin *et al.* (1996) and the references therein]. Compared to this, relatively little attention has been paid so far to circular motions of cylinders in fluids. Also, for such a flow situation there are important practical applications as, for instance, stirrers used in the chemical industry for mixing or long flexible shafts rotating in fluids. To the authors' knowledge the only work dealing with such a flow configuration is that in Chaplin (1988), where a cylinder orbitally moving (without rotation) in a planar oscillatory infinite fluid is studied, and in Wu & Sheridan (1997), where a cylinder orbiting in a confined fluid is investigated experimentally.

The flow situation considered in the present paper is similar to that in Wu & Sheridan (1997): a cylinder orbiting on a circular trajectory within a large vessel filled with fluid. The corresponding problem configuration is indicated in Figure 1. During the orbital movement the points on the cylinder keep their position relative to the orbit centre. As it is well known, above some critical Reynolds number a cylinder moving in a fluid generates the classical Kármán vortex street (see Figure 2). Moving on a circular trajectory the cylinder successively may run through its own wake, resulting in more and more complex flow patterns. The objective of the present study is the determination of the general flow behaviour for this kind of flow situation and the examination of the influence of characteristic problem

0889–9746/02/040435 + 17 $35.00/0

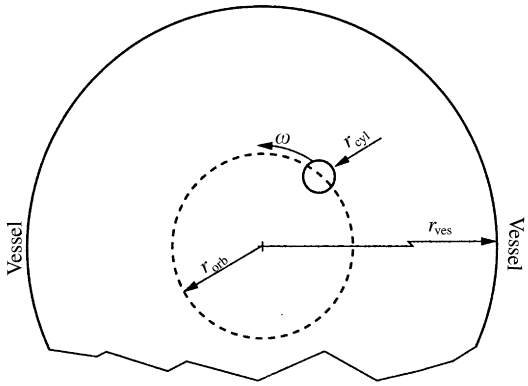

Figure 1. Problem configuration.

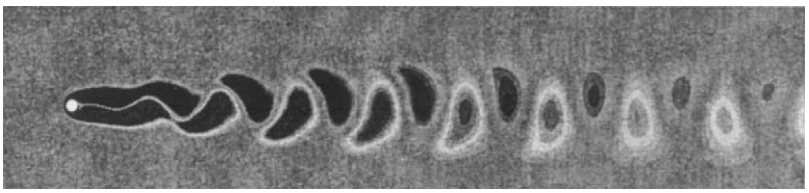

Figure 2. Kármán vortices.

parameters, such as the angular velocity ω, the cylinder radius r_{cyl} and the orbit radius r_{orb}. The problem is studied by numerical simulation. In order to obtain numerically reliable results, the influence of numerical parameters, such as the number of grid points and the time-step size on the quality of the predictions is investigated. A reference set of problem parameters is fixed, serving as a basis for the adjustment of the numerical parameters. Some simplifying assumptions are made in order to limit the complexity of the problem. The flow is regarded as two-dimensional and the fluid is assumed to be an incompressible Newtonian one with constant fluid properties. Only laminar flow regimes with a maximum Reynolds number of about 100 are considered. The vessel radius is chosen to be fairly large compared to the orbit radius, such that the vessel wall has no significant influence on the flow field in the region of the orbiting cylinder.

2. GOVERNING EQUATIONS

With respect to a Cartesian coordinate system with origin at the centre of the orbit (see Figure 1) the orbital movement of the cylinder can be described by the equation of motion

$$\mathbf{x}(t) = r\cos(\omega t)\mathbf{e}_1 + r\sin(\omega t)\mathbf{e}_2. \tag{1}$$

where $\mathbf{e}_1$ and $\mathbf{e}_2$ are the Cartesian unit basis vectors, $\mathbf{x}$ is the position vector, t is the time, ω is the angular velocity and r is the distance of a point on the cylinder from the origin of the orbit. Note that for any point on the cylinder r is fixed during the motion and is bounded by

$$\max\{0, r_{\mathrm{orb}} - r_{\mathrm{cyl}}\} \leq r \leq r_{\mathrm{orb}} + r_{\mathrm{cyl}}. \tag{2}$$

The velocity of the points on the cylinder is given by

$$\mathbf{v}(t) = \frac{\mathrm{d}\mathbf{x}}{\mathrm{d}t} = -r\omega \sin(\omega t)\mathbf{e}_1 + r\omega \cos(\omega t)\mathbf{e}_2. \tag{3}$$

The velocity of the centre of the cylinder, i.e., equation (3) with $r = r_{\mathrm{orb}}$, which will be used for the definition of the Reynolds number, we denote by $\mathbf{v}_{\mathrm{cyl}}$.

The considered flow problem can be described by the balance equations for mass and momentum for an incompressible Newtonian fluid with constant fluid properties. In a stationary frame of reference these equations can be written as

$$\nabla \cdot \mathbf{u} = 0, \qquad \rho \frac{\mathrm{D}\mathbf{u}}{\mathrm{D}t} - \nabla \cdot \mathbf{T} = 0, \tag{4), (5}$$

where ρ is the fluid density, $\mathbf{u} = \mathbf{u}(\mathbf{x}, t)$ is the velocity vector, $\mathrm{D}/\mathrm{D}t$ is the material derivative and ∇ is the gradient operator with respect to the spatial coordinates. The stress tensor $\mathbf{T}$ is defined by

$$\mathbf{T} = -p\mathbf{I} + \mu(\nabla \mathbf{u} + \nabla \mathbf{u}^{\mathrm{T}}), \tag{6}$$

with the dynamic viscosity μ, the pressure $p = p(\mathbf{x}, t)$ and the unity tensor $\mathbf{I}$.

The use of the balance equations in the above form, i.e., in a stationary frame of reference, would be disadvantageous for the numerical treatment of the considered problem configuration, since it would require the use of deforming numerical grids together with rather complicated boundary conditions. A more convenient approach is to transform the equations into a suitable moving reference system, such that relative to this system the grid and the boundary conditions can be handled in an easier way. In general, for a reference system rotating with an angular velocity $\boldsymbol{\Omega}$ and translating with a velocity $\mathbf{c}$ (velocity of the origin) equations (4) and (5) transform into the equations [see, e.g., Spurk (1989)]:

$$\nabla \cdot \tilde{\mathbf{u}} = 0, \tag{7}$$

$$\rho \frac{\mathrm{D}\tilde{\mathbf{u}}}{\mathrm{D}t} - \nabla \cdot \mathbf{T} = -\rho \left[\frac{\mathrm{D}\mathbf{c}}{\mathrm{D}t} + 2\boldsymbol{\Omega} \times \tilde{\mathbf{u}} + \frac{\mathrm{D}\boldsymbol{\Omega}}{\mathrm{D}t} \times \mathbf{x} + \boldsymbol{\Omega} \times (\boldsymbol{\Omega} \times \mathbf{x}) \right]; \tag{8}$$

$\tilde{\mathbf{u}}$ is the velocity relative to the moving system, which is related to $\mathbf{u}$ by

$$\tilde{\mathbf{u}} = \mathbf{u} - \boldsymbol{\Omega} \times \mathbf{x} - \mathbf{c}. \tag{9}$$

While the continuity equation (7) remains unchanged, due to volume forces resulting from the acceleration and the rotation of the frame of reference, additional terms appear in the momentum equations (8): the acceleration of the reference system $\mathrm{D}\mathbf{c}/\mathrm{D}t$, the Coriolis acceleration $2\boldsymbol{\Omega} \times \tilde{\mathbf{u}}$, the angular acceleration $(\mathrm{D}\boldsymbol{\Omega}/\mathrm{D}t) \times \mathbf{x}$ and the centrifugal acceleration $\boldsymbol{\Omega} \times (\boldsymbol{\Omega} \times \mathbf{x})$.

For our problem configuration one can think of special moving reference systems which might be useful to handle the problem: the system which rotates around the centre of the orbit (rotational system), with the orbiting cylinder located eccentrically but in the centre of the grid. The system is illustrated in Figure 3. Three cylinder positions for different times are sketched, showing that the grid is tightly mounted to the cylinder and follows the orbiting movement around the centre of the vessel. Since the origin of the rotating coordinate system remains fixed in the centre of the vessel, we have no translational velocity ($\mathbf{c} = \mathbf{0}$). The rotational velocity is $\boldsymbol{\Omega} = \omega \mathbf{e}_3$, such that the momentum equations (8) can be written:

$$\rho \frac{\mathrm{D}\tilde{\mathbf{u}}}{\mathrm{D}t} - \nabla \cdot \mathbf{T} = -\rho [2\boldsymbol{\Omega} \times \tilde{\mathbf{u}} + \boldsymbol{\Omega} \times (\boldsymbol{\Omega} \times \mathbf{x})].$$

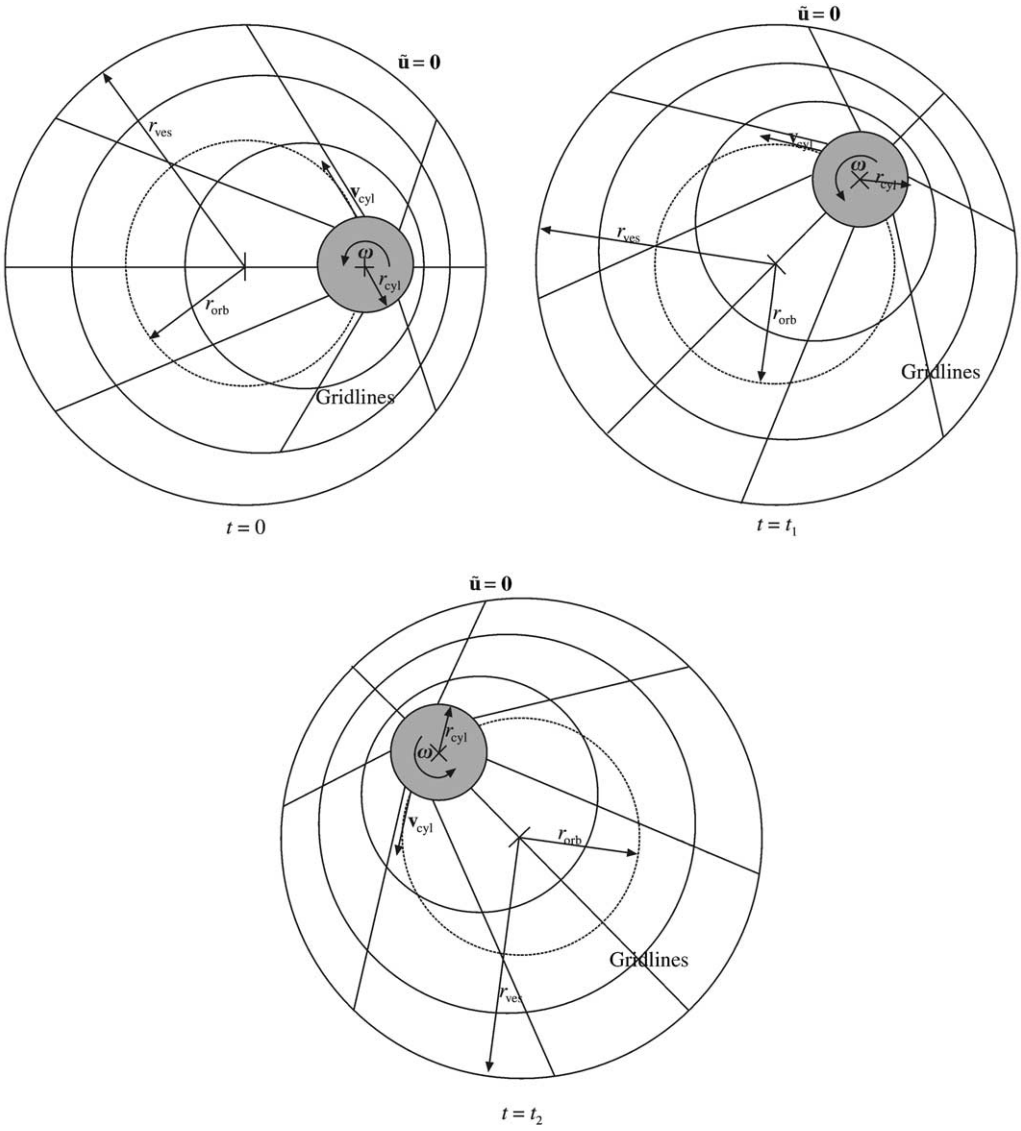

Figure 3. Rotational reference system.

To avoid the movement of the grid, additionally, for the actual computations, we look at the problem from a reverse point of view, i.e., the cylinder and the grid remain fixed at a certain position and the outer vessel boundary moves instead with corresponding negative velocity. In this case accurate boundary conditions can be applied easily (see Figure 4): $\tilde{\mathbf{u}}_{\text{ves}} = -\boldsymbol{\Omega} \times \mathbf{x}_{\text{ves}}$ at the vessel wall and $\tilde{\mathbf{u}}_{\text{cyl}} = \mathbf{0}$ at the cylinder surface. We emphasize that imposing these conditions the considered problem configuration is represented exactly. All numerical results reported in the next section, are obtained on the basis of this problem setting.

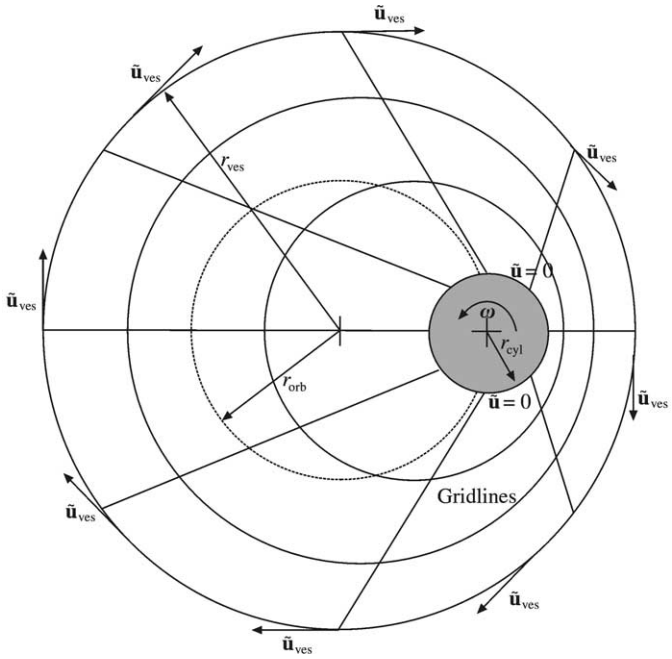

Figure 4. Boundary conditions in the rotational frame of reference.

In order to identify the characteristic parameters of the flow we introduce dimensionless values for the coordinate $\mathbf{x}$, the velocity $\tilde{\mathbf{u}}$, the pressure p and the time t in the following way:

$$\mathbf{x}^* = \frac{\mathbf{x}}{r_{cyl}}, \quad \mathbf{u}^* = \frac{\tilde{\mathbf{u}}}{|\mathbf{v}_{cyl}|}, \quad p^* = \frac{p}{\rho \mathbf{v}_{cyl}^2}, \quad t^* = \frac{|\mathbf{v}_{cyl}|t}{r_{cyl}}.$$

With this, after introducing the stress tensor (6) and some simple algebra, the momentum equations (8) can be written in the following dimensionless form:

$$\frac{\mathrm{D}\mathbf{u}^*}{\mathrm{D}t^*} + \nabla^* p^* - \frac{\mu}{\rho |\mathbf{v}_{cyl}| r_{cyl}} \Delta^* \mathbf{u}^* = -2\frac{\omega r_{cyl}}{|\mathbf{v}_{cyl}|}[\mathbf{e}_3 \times \mathbf{u}^*] - \left(\frac{\omega r_{cyl}}{|\mathbf{v}_{cyl}|}\right)^2 [\mathbf{e}_3 \times (\mathbf{e}_3 \times \mathbf{x}^*)]. \quad (10)$$

Introducing a Reynolds number defined by

$$\mathrm{Re} = \frac{2 r_{cyl} |\mathbf{v}_{cyl}| \rho}{\mu} \quad (11)$$

and a Keulegan–Carpenter number defined by

$$\mathrm{KC} = \frac{|\mathbf{v}_{cyl}|}{\omega r_{cyl}} = \frac{r_{orb}}{r_{cyl}}, \quad (12)$$

equation (10) takes the form

$$\frac{\mathrm{D}\mathbf{u}^*}{\mathrm{D}t^*} + \nabla^* p^* - \frac{2}{\mathrm{Re}} \Delta^* \mathbf{u}^* = -\frac{2}{\mathrm{KC}}[\mathbf{e}_3 \times \mathbf{u}^*] - \frac{1}{\mathrm{KC}^2}[\mathbf{e}_3 \times (\mathbf{e}_3 \times \mathbf{x}^*)]. \quad (13)$$

It can be seen that, if the influence of the far-field radius is neglected, the problem features are fully described by the two dimensionless parameters Re and KC.

For the monitoring of the temporal behaviour of the results in the next sections a further dimensionless quantity is introduced: the lift coefficient c_L for the cylinder defined by

$$c_L = \frac{-1}{\rho |\mathbf{v}_{\mathrm{cyl}}|^2 r_{\mathrm{cyl}}} \int_S \left(\mu \frac{\partial \mathbf{u}_t}{\partial \mathbf{n}} n_1 + p n_2 \right) \mathrm{d}S, \tag{14}$$

with the cylinder surface S, the outwards normal vector $\mathbf{n} = n_1 \mathbf{e}_1 + n_2 \mathbf{e}_2$ on S and the tangential velocity $\mathbf{u}_t$. The lift coefficient defined in this way is a measure of the radial force affecting the cylinder. For the visualization of the flow patterns the vorticity ζ defined by

$$\nabla \times \mathbf{u} = \zeta \mathbf{e}_3 = \left(\frac{\partial u_2}{\partial x_1} - \frac{\partial u_1}{\partial x_2} \right) \mathbf{e}_3 \tag{15}$$

is considered, which easily allows to identify shedding and motion of vortices.

3. NUMERICAL METHOD AND NUMERICAL ACCURACY

Concerning the numerical solution procedure employed we only give a brief summary and refer to Durst & Schäfer (1996) for a detailed description. The equations are discretized using a fully conservative finite-volume method on block-structured boundary-fitted grids. In total, the order of accuracy of the spatial discretization scheme is about 1·5 due to the usage of a mixture of the second order central differencing approximation and the upwind scheme of first order for flux interpolations (flux-blending technique with factor 0·5). The applied temporal discretization scheme is the three-point-backward method, which is second-order accurate. A global nonlinear multi-grid technique with a pressure correction approach of SIMPLE-type acting as smoother and coarse grid solver is used for the solution of the discretized coupled system of equations for each time step.

Before systematically studying the physical problem, some test computations were carried out in order to fix the requirements of the numerical resolution. Here, the major objective was to ensure that the grid size (number of cells n_{cell}) and the time-step size Δt are adjusted properly such that reliable results with reasonable computational effort can be achieved.

For this, first a reference set of problem parameters (as given in Table 1) has been fixed, for which this adjustment was carried out. For this set (highest considered Re-number and the lowest considered KC-number) we expect the highest flow pattern complexity and the highest disturbance of the cylinders wake. It is therefore the most critical combination from the numerical point of view. Results for the reference case were computed with successively refined grids (by a factor of 4) and time-step sizes (by a factor of 2). As a measure of accuracy the temporal variation of the lift coefficient c_L for the cylinder was taken. Figure 5 shows the results for grids with cell numbers n_{cell} of 128×128, 256×256 and 512×512 with a fixed time-step size of $\Delta t = 0.01$ s. After an unordered starting period the lift shows a regular oscillating behaviour with declining amplitude and frequency on all grids. A higher spatial resolution leads to higher amplitudes and frequencies. However, these quantities strongly depend on the spatial discretization, however the mean level does not. Figure 6 shows the results for different time-step sizes of $\Delta t = 0.01$, 0.005 and 0.0025 s for a fixed spatial discretization with $n_{\mathrm{cell}} = 128 \times 128$. One can see that, compared to the results with $\Delta t = 0.005$ s, there are considerable differences in the results with $\Delta t = 0.01$ s, while with $\Delta t = 0.0025$ s the improvement in accuracy is not very significant.

Taking into account the computing times necessary for the different numerical resolutions, which due to the multigrid technique employed increases closely linearly with n_{cell} and the number of time steps (which means that the solution method can be viewed as

TABLE 1
Parameter set for reference case

Problem parameter	Reference value
Angular velocity, ω	$4\,\pi$/s
Orbit radius, r_{orb}	0.1 m
Cylinder radius, r_{cyl}	0.02 m
Vessel radius, r_{ves}	2 m
Fluid density, ρ	1 000 kg/m^3
Fluid viscosity, μ	0.44 Ns/m^2
Reynolds number Re	114
Keulegan–Carpenter number KC	5

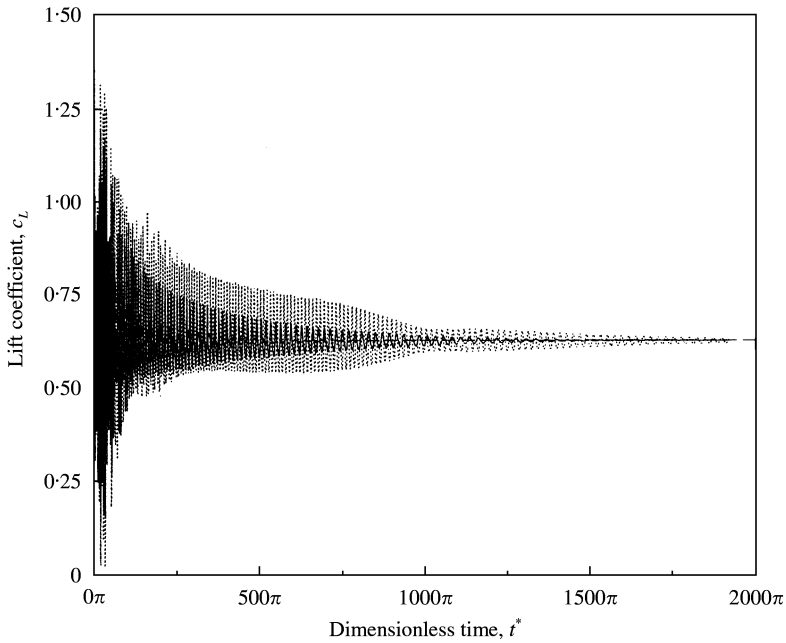

Figure 5. Lift history for different grid sizes: – – –, grid 6: 128 × 128 cv; ——, grid 7: 256 × 256 cv; · · · · · ·, grid 8: 512 × 512 cv.

rather efficient), we have to find a reasonable compromise between accuracy and computational effort. In particular, the high amount of time steps (due to the requirement of a large real time) leads to enormous computing times in the range of months for the grid with $n_{cell} = 512 \times 512$ even on a parallel cluster system of Pentium III processors. As a compromise, further calculations have been performed with $n_{cell} = 256 \times 256$ and $\Delta t = 0.005$ s, always having in mind the limited spatial accuracy, which, however, is not that critical with respect to our major purpose, i.e., to study the influence of the Re- and KC-numbers on the flow properties.

Another preliminary test computation was carried out to check the influence of the vessel radius r_{ves} on the flow field, which we would like to be not very significant in order to concentrate on the effects induced by the orbiting cylinder without much disturbance from other effects. Here, the case Re = 57 and KC = 10 was considered. The results of three

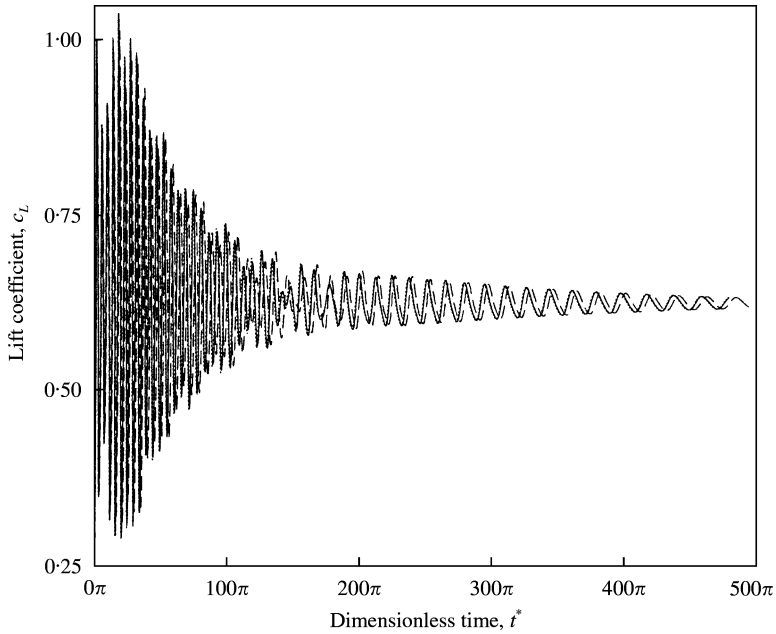

Figure 6. Lift history for different time-step sizes: – – –, $\Delta t = 2.5 \times 10^{-3}$; ——, $\Delta t = 5.0 \times 10^{-3}$; · · · · · ·, $\Delta t = 10^{-2}$.

different radii ratios were compared:

$$R_v = \frac{r_{\text{ves}}}{r_{\text{orb}}} = [5;\ 10;\ 20].$$

Figure 7 shows the variation of the lift coefficient for the three cases. While we find significant differences in comparison of the small- and middle-sized radius, only small differences occur between the middle and large vessel radius with regard to amplitude and frequency of the oscillation. The value $R_v = 10$ is assumed to be large enough for our purpose. All computations reported in the next section are performed with this value.

4. NUMERICAL RESULTS

The major objective of this work is to investigate the nature of the flow field related to the considered problem configuration and to study how the variation of the characteristic problem parameters influence the results. The dimensionless form of the momentum equation (13) expresses, that the flow only depends on the dimensionless Re-number and KC-number. We consider the following variations of these two numbers:

$$\text{Re} = [28.5;\ 57;\ 114] \quad \text{and} \quad \text{KC} = [5;\ 10;\ 20],$$

which appeared as reasonable settings for nonturbulent flows. In combination this leads to a variety of nine different flow cases. We examine the influence of the dimensionless numbers on the flow field by observing the temporal developement of the lift coefficient c_L. Figure 8 shows the lift history for Re = 57 and varying values of the KC-number. One can observe that at the beginning of the rotational process, the interference of the actually shed vortices with the "old" ones of the dissipating wake of previous cylinder revolutions leads to

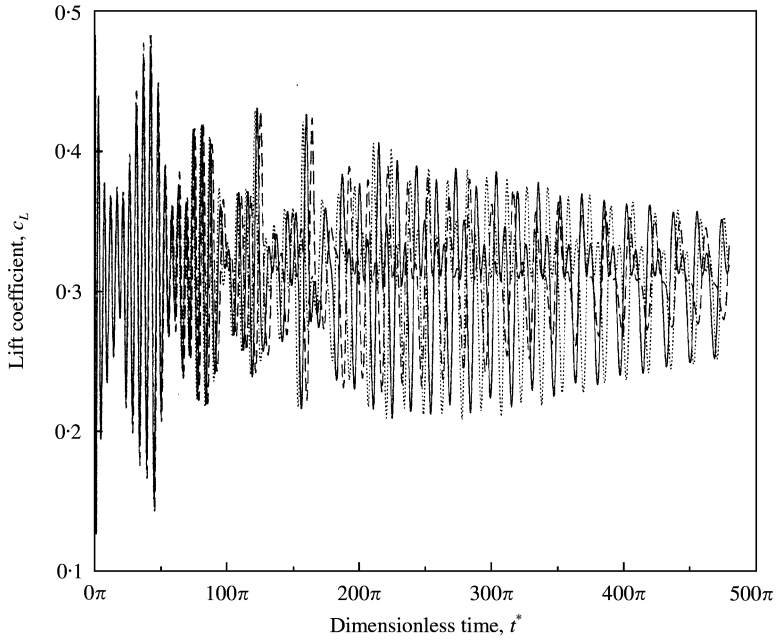

Figure 7. Lift history for different ratios of vessel and orbit radii R_v: – – –, $R_v = 5$; ——, $R_v = 10$; · · · · · ·, $R_v = 20$.

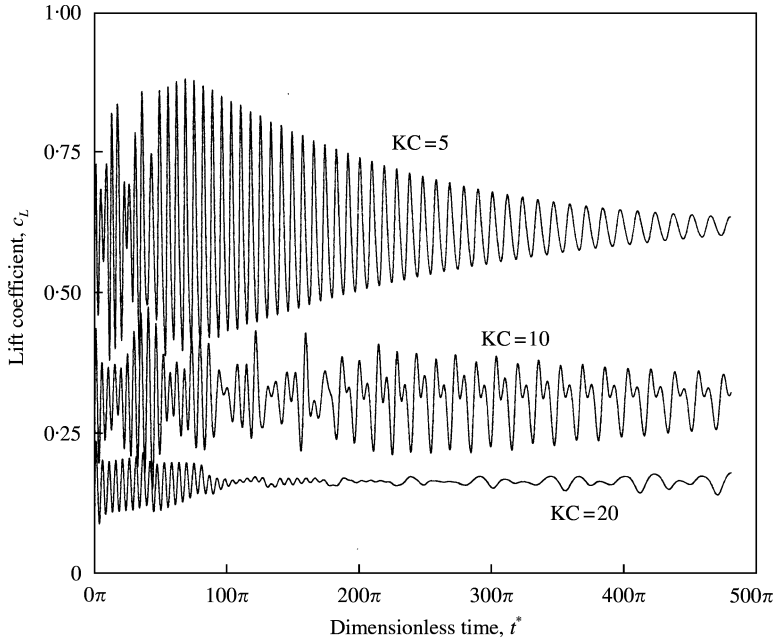

Figure 8. Lift history for Re = 57 and different KC-numbers.

nonharmonic vortex structures. Rather, harmonic oscillations of the lift for the smallest KC-number are found, which means that the flow pattern is dominated by the actual vortex separation with only small disturbance of the "previous" flow fields.

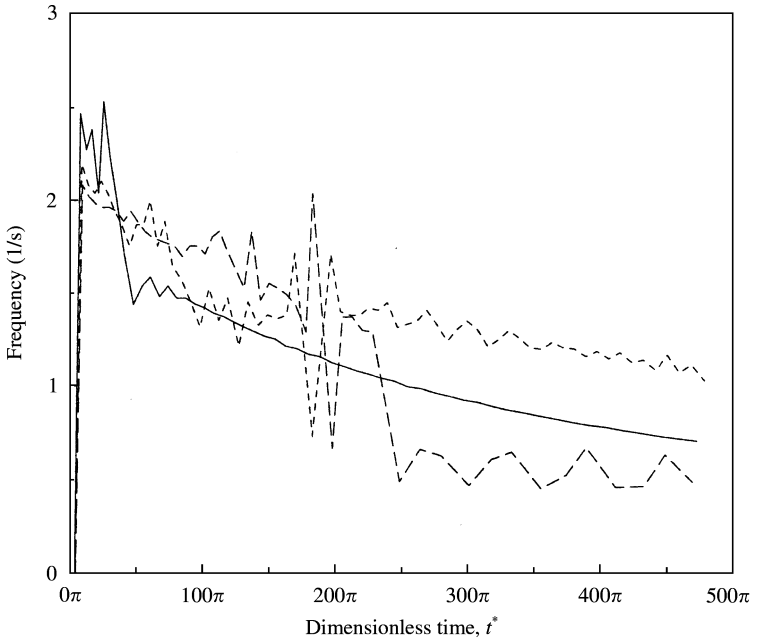

Figure 9. Frequency history for Re = 57 and different KC-numbers: ——, KC = 5; - - -, KC = 10; – – –, KC = 20.

Taking a look at the long-term behaviour of the levels of the lift values, we find a reciprocal relation to the KC-number. This is in accordance with the *Kutta–Joukowsky theorem* stating that for a cylinder moving in a fluid, the lift force A is proportional to the circulation Γ and the characteristic velocity u_∞ (Spurk 1989):

$$A = -\rho \Gamma u_\infty. \tag{16}$$

Taking into account that Γ is proportional to ω and u_∞ depending linearly on $|\mathbf{v}_{\mathrm{cyl}}|$, we can deduce

$$A \sim \omega |\mathbf{v}_{\mathrm{cyl}}| = \omega^2 r_{\mathrm{orb}}.$$

Combining the definitions for the Re- and KC-number we obtain

$$\omega \sim \frac{\mathrm{Re}}{\mathrm{KC}} \quad \text{and} \quad r_{\mathrm{orb}} \sim \mathrm{KC} \quad \Rightarrow \quad |\mathbf{v}_{\mathrm{cyl}}| \sim \frac{1}{\mathrm{Re}},$$

yielding the following estimate for the lift force:

$$A \sim \frac{\mathrm{Re}^2}{\mathrm{KC}^2}\mathrm{KC} = \frac{\mathrm{Re}^2}{\mathrm{KC}}.$$

Substituting this into equation (14) gives the relation

$$c_L = \frac{-A}{\rho |\mathbf{v}_{\mathrm{cyl}}|^2 r_{\mathrm{cyl}}} \sim \frac{1}{\mathrm{KC}} \tag{17}$$

under the assumption that $\mathrm{KC} \geq 1$. This reciprocal dependence of the relation between the lift coefficient and the dimensionless KC-number is in accordance with the results of

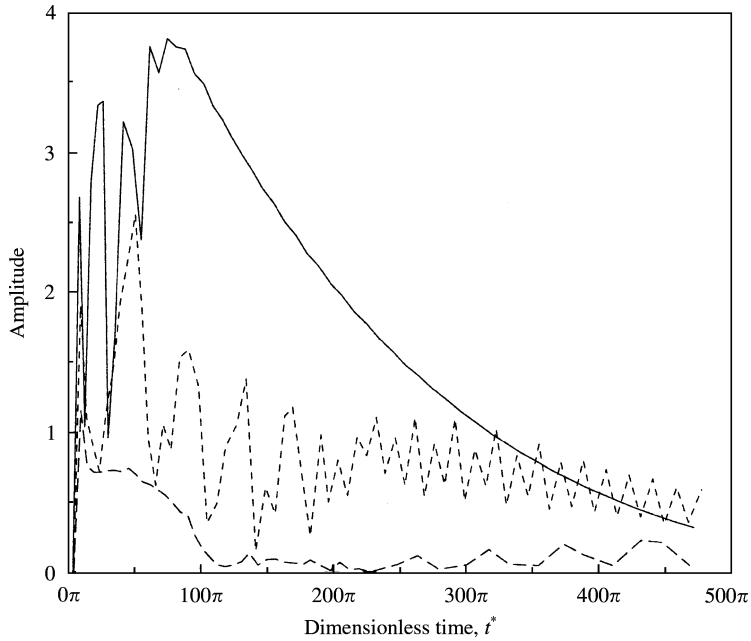

Figure 10. Amplitude history for Re = 57 and different KC-numbers: ——, KC = 5; - - -, KC = 10; – – –, KC = 20.

TABLE 2
Comparison of analytical and numerical lift coefficients

	Analytical value of c_L	Numerical value of c_L
KC = 5	0·628	0·616
KC = 10	0·314	0·332
KC = 20	0·157	0·156

Figure 8. Thus, the lift coefficient level is independent of the Re-number and therefore of the rotational velocity.

To get a more clear picture of the oscillating character of the lift, the histories of the frequencies and amplitudes are shown in Figures 9 and 10. As already pointed out before, after an inharmonic starting period with strong frequency and amplitude variations, we find rather uniform oscillations related to regular separation of vortices with only small disturbances from previous rotations. Another effect that can be observed is the decrease of the oscillations of the lift with time, which means that the vortices dissipate completely and the separation of new ones terminates. From revolution to revolution the whole fluid in the vessel is set in motion until it rotates with the same velocity as the cylinder (like when stirring fluid in a cup). With the reduction of the relative velocity the frequency of the vortex shedding decreases as well as the lift amplitudes, which turns out very clearly for the KC = 5 case. At the state of a uniformly moving fluid only the centrifugal force

$$F_{\text{centr}} = -ma = -\omega^2 r_{\text{orb}} \rho \pi r_{\text{cyl}}^2$$

with m denoting the mass and a the acceleration acts on the cylinder which equals the stress forces. Therefore, we find a rather constant value for the long-term lift coefficient, which can

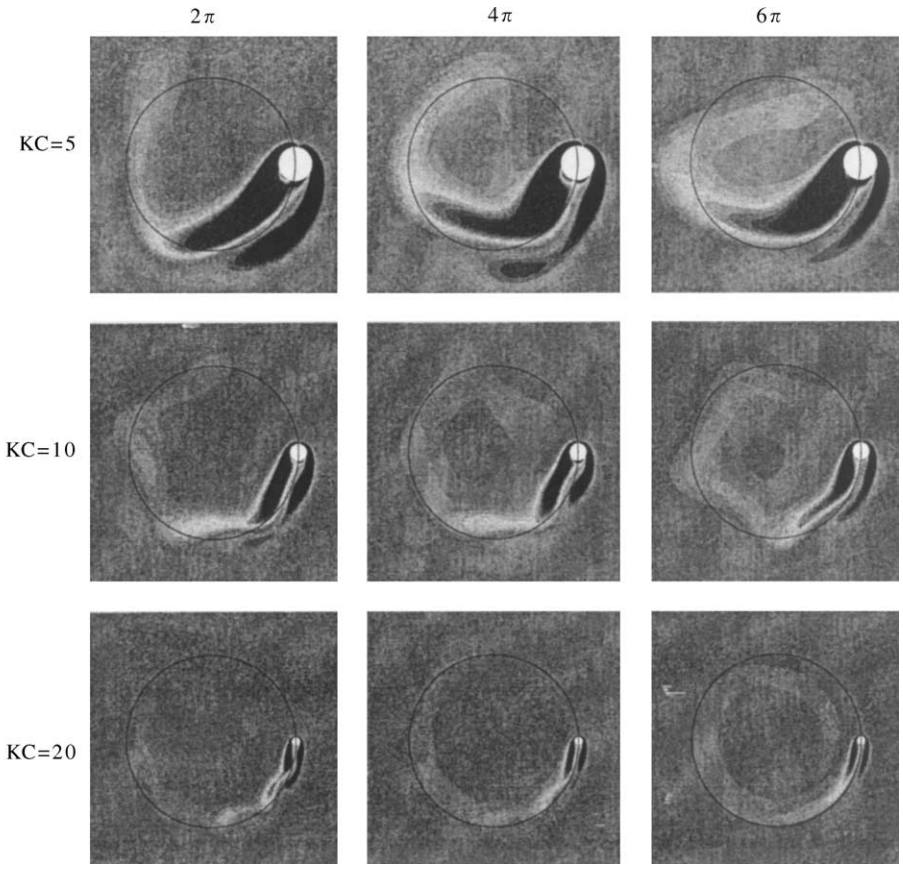

Figure 11. Vorticity field for Re = 57 and different KC-numbers after one, two and three revolutions.

easily be derived from the lift definition

$$c_L = \frac{-F_{\text{centr}}}{\rho|\mathbf{v}_{\text{cyl}}|^2 r_{\text{cyl}}} = \frac{\omega^2 r_{\text{orb}} \rho \pi r_{\text{cyl}}^2}{\rho|\mathbf{v}_{\text{cyl}}|^2 r_{\text{cyl}}}.$$

This finally yields

$$c_L = \frac{\pi r_{\text{cyl}}}{r_{\text{orb}}} = \frac{\pi}{\text{KC}}, \tag{18}$$

which is in accordance with the numerical results. In Table 2, the numerical lift values are compared to the analytical ones taken from equation (18). Because for the presented cases the stadium of a uniformly moving fluid is not yet fully reached, we extrapolated the long-term lift coefficients from the average value of the last oscillations. We obtain a very good agreement of the values for all three KC-numbers.

To get an impression of the nature of the flow field, Figure 11 presents the vorticity of the fluid flow after one, two and three completed revolutions for all three KC-numbers. Note that different KC-numbers mean different orbit radii, such that a constant clipping leads to decreasing cylinder sizes.

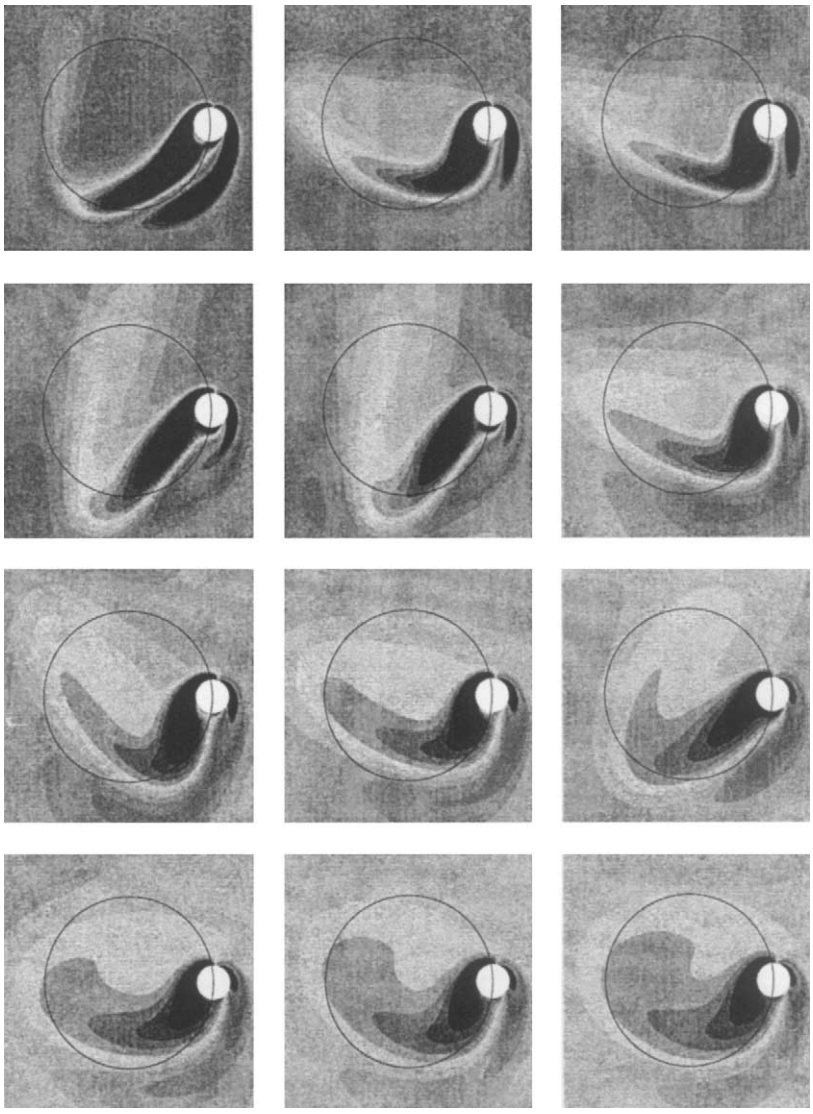

Figure 12. Vorticity field for long-term history for Re = 57 and KC = 5 after each fourth revolution (from left to right).

Furthermore, a long-term development of the flow is considered in Figure 12, where for KC = 5, the vorticity for each fourth revolution is given. The described effects of declining frequencies of vortex separation and of the relative velocity are seen to materialize.

For the other Re-numbers we find very similar effects. Admittedly, for Re = 114 (see Figures 13–15) the amplitudes and frequencies of the oscillations of the starting period are much larger than for the Re = 57. However, after several revolutions with strong wake interference forming disturbed complicated flow patterns, one can observe that the lift develops again regularly. Again, the smallest KC-number yields the most harmonic oscillations monotonically decreasing in frequency and amplitude. For the other KC-numbers an interference of oscillations occur after some time resulting in a more disturbed vortex

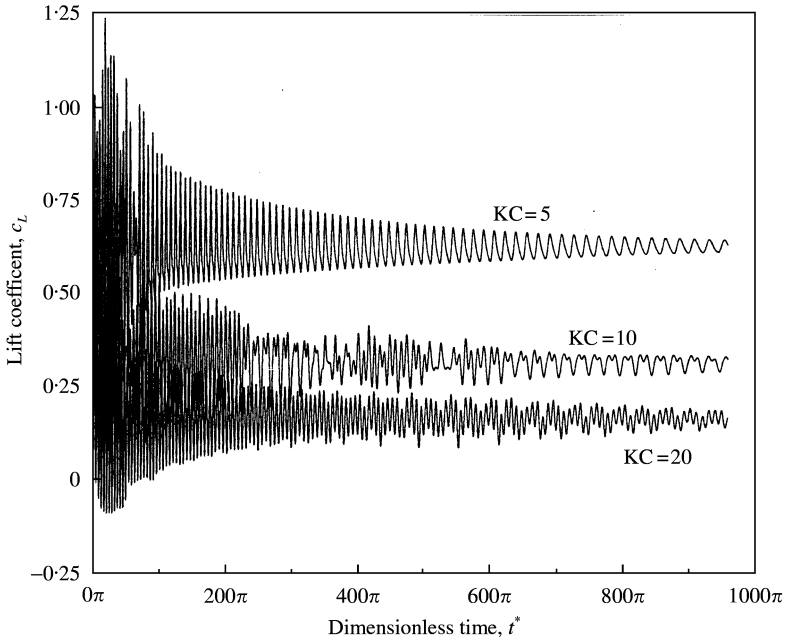

Figure 13. Lift history for Re = 114 and different KC-numbers.

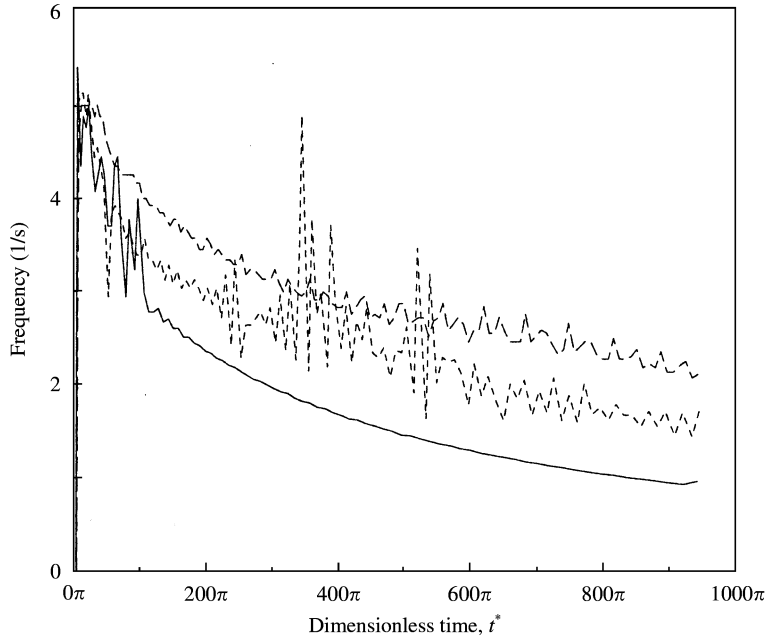

Figure 14. Frequency history for Re = 114 and different KC-numbers: ——, KC = 5; - - -, KC = 10; – – –, KC = 20.

shedding with varying lift frequencies. Nevertheless, the amplitude and frequency decrease continuously.

As expected, vortices are shed much slower for the smallest Re-number investigated (Figures 16–18). Due to this, amplitudes and frequencies are accordingly smaller compared

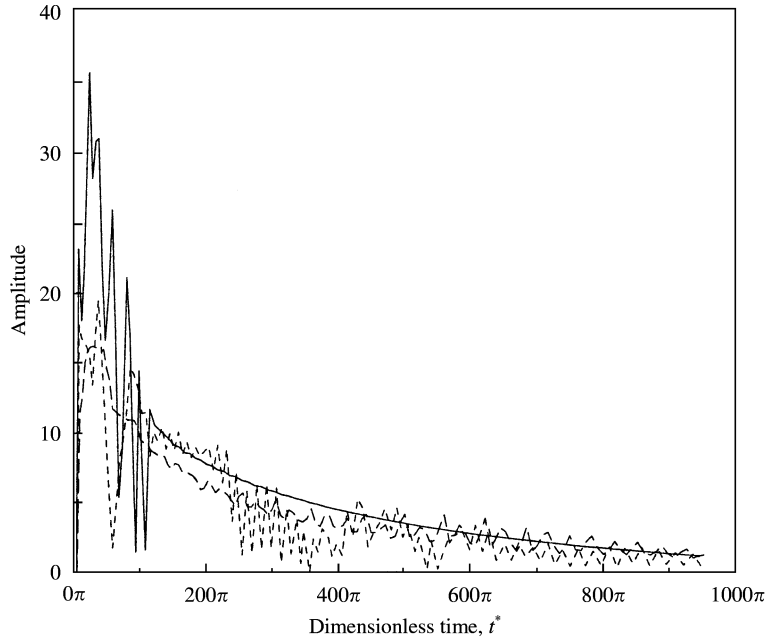

Figure 15. Amplitude history for Re = 114 and different KC-numbers: ——, KC = 5; - - -, KC = 10; – – –, KC = 20.

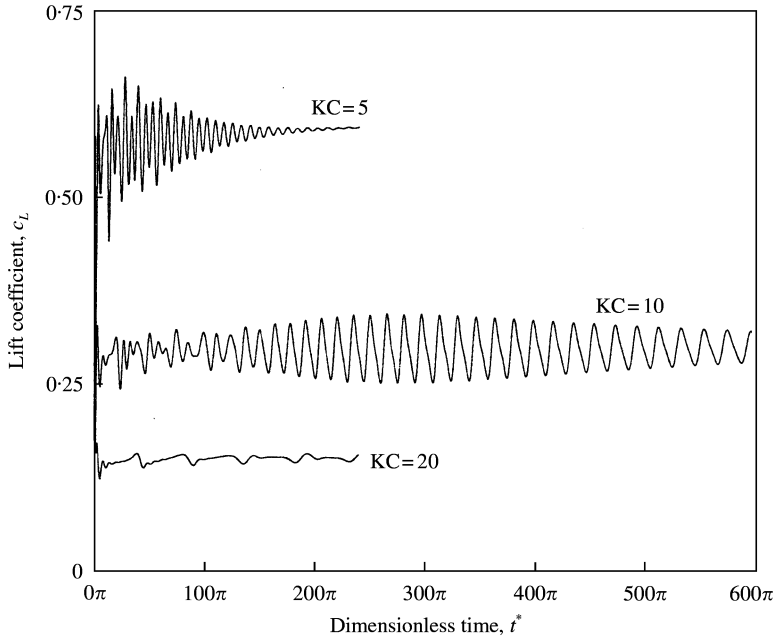

Figure 16. Lift history for Re = 28.5 and different KC-numbers.

to the higher Re-numbers. For KC = 20 almost all vortices are already dissipated before they can interfere with the new flow pattern of the next revolution. Lift oscillations can hardly be observed for this case. During the whole temporal period, the rate of vortex

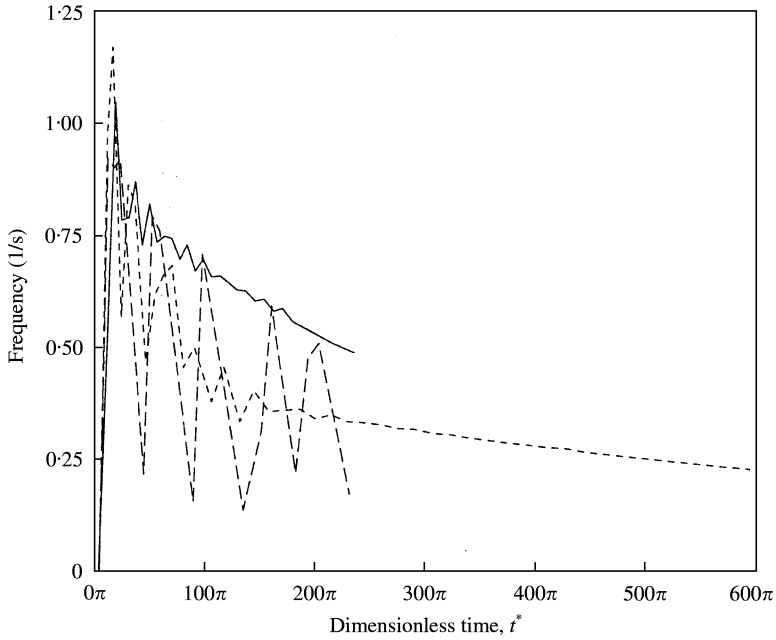

Figure 17. Frequency history for Re = 28.5 and different KC-numbers: ——, KC = 5; - - -, KC = 10; – – –, KC = 20.

shedding in this case is very low due to the large ratio between cylinder and orbit radii. "Previous" flow fields only slightly influence the actual one. However, we find remarkably different results for KC = 10. After a starting period with an nonharmonic lift development, the frequency of the vortex shedding stabilizes and vortices separate harmonically but with slightly increasing amplitudes. Further investigations showed that this state of the flow continues for a rather long time before the reduction of amplitudes and frequencies prevail again. It takes much more time compared to the other cases to yield the vessel fluid being fully in motion. We can conclude that this behaviour is due to a kind of resonance between the old and dissipating wake of a former revolution and the actual separated vortices of the new revolution.

Taking the results for all Re-numbers into account, we find, that the theoretical independence of the long-term lift coefficient from Re, which was derived in equations (17) and (18), is fully recovered. Only slight deviations of the average lift show up for varying Re- at constant KC-numbers.

5. CONCLUSIONS

We have presented results of flow simulations for a cylinder orbiting in a fluid, where special attention has been paid to the variation of the flow pattern when varying the KC- and Re-number, which are the important problem parameters.

The dependence of numerical parameters such as time-step size and grid resolution was investigated first, leading to a reasonable numerical setting from the accuracy point of view for further investigations. In particular, it turned out that the problem configuration is rather demanding with respect to the spatial resolution in order to get numerical results with adequate accuracy.

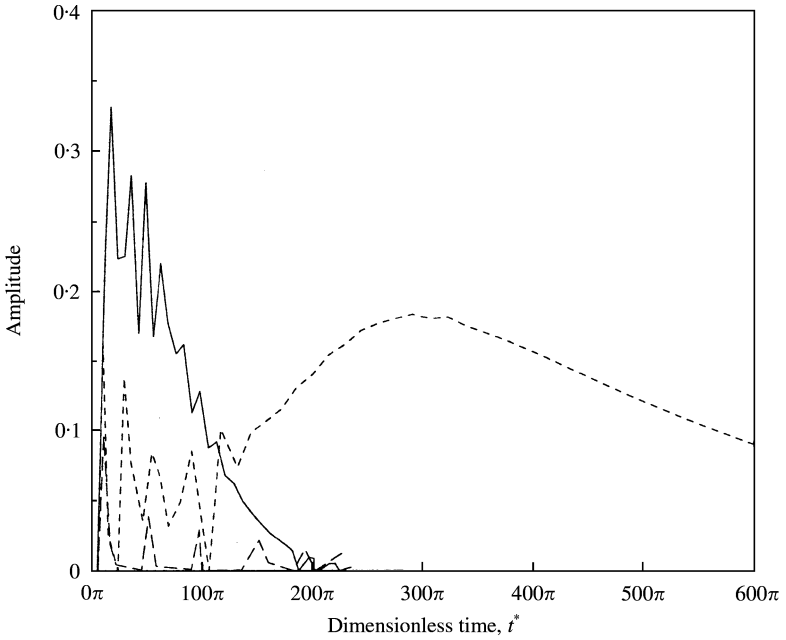

Figure 18. Amplitude history for Re = 28.5 and different KC-numbers: ——, KC = 5; - - -, KC = 10; – – –, KC = 20.

We found the lift coefficient in the long-term depending only on the KC-number. The Re-number just influences the amplitudes of the oscillations of the nonregular starting period, where very complex flow structures develop. Due to the influence of the vessel boundary the amplitudes and frequencies decrease in time until fluid and cylinder move with the same velocity. For small Re-numbers this flow state is reached after a shorter period of dimensionless time. For KC = 5 all computations showed a history of very regularly shed Kármán-vortices, while for the larger KC-numbers the interference of previous and new vortices lead to more nonharmonic flow structures and lift oscillations.

References

CHAPLIN, J.R. 1988 Loading on a cylinder in uniform oscillatory flow. Part I — planar oscillatory flow. *Applied Ocean Research* **10**, 120–128.

DURST, F. & SCHÄFER, M. 1996 A parallel blockstructured multigrid method for the prediction of incompressible flows. *International Journal for Numerical Methods in Fluids* **22**, 549–565.

DÜTSCH, H., DURST, F., BECKER, S. & LIENHART, H. 1998 Low-Reynolds-number flow around an oscillating circular cylinder at low Keulegan–Carpenter numbers. *Journal of Fluid Mechanics* **360**, 249–271.

LIN, X., BEARMAN, W. & GRAHAM P.W. 1996 A numerical study of oscillatory flow about a circular cylinder for low values of beta parameters. *Journal of Fluids and Structures* **10**, 501–526.

SPURK, J. 1989 *Strömungslehre*. Berlin: Springer.

TATSUNO M. & BEARMAN P.W. 1990 A visual study of the flow around an oscillating circular cylinder at low Keulegan–Carpenter numbers and low stokes numbers. *Journal of Fluid Mechanics* **211**, 159–171.

WU, J. & SHERIDAN, J. 1997 The wake of an orbiting cylinder. *Journal of Fluids Structures* **11**, 617–626.

ZDRAVKOVICH, M. M. 1997 *Flow Around Circular Cylinders*. Vol.1: *Fundamentals*. Oxford: Oxford University Press.